BNL-8497

Heat Transfer to Liquid Metals Flowing Turbulently in Eccentric Annuli*

by

Wen-Shi Yu

and

Orrington E. Dwyer

October 7, 1964

(Submitted to A.I.Ch.E. for presentation at the Houston Meeting, February 1965, and later to be submitted to A.N.S. for publication in Nuclear Science and Engineering.)

Number of copies submitted:

Number of manuscript pages: 35

Number of figures: 17

Number of tables: 3

*This paper is based on a thesis carried out at the Brookhaven National Laboratory by Miss Wen-Shi Yu for the Ph.D. degree in Chemical Engineering from the Polytechnic Institute of Brooklyn, June 1964. The work was sponsored by the U. S. Atomic Energy Commission.

DISCLAIMER

ABSTRACT

An analytical study was carried out to determine the effects of the degree of eccentricity of the two circles of an annulus on both local and average heat transfer coefficients for turbulent flow of liquid metals. The study was based on the conditions of (a) heat transfer to or from the inner wall only, (b) uniform heat flux, and (c) fully developed temperature and velocity profiles. The scope of the investigation is indicated by the following ranges of parameters studied:

Reynolds number, 5×10^4 to 10^6

Peclet number, 360 to 8000

Ratio of outer to inner radius, 1.0 to 4.0

Eccentricity, up to 70% of maximum displacement

The results showed that eccentricity can have very great effects on both the local and average heat transfer coefficients and consequently on the circumferential temperature variations around the annulus walls. At a radius ratio of 1.5 and a Peclet number of 1700, for example, the average coefficient was found to decrease 63 and 93%, when the eccentricity was increased from 0.0 to 0.30 and from 0.0 to 0.70, respectively. Under these conditions, the ratios of total circumferential temperature difference to the difference between the average inner wall temperature

and the stream bulk temperature were found to be 3.20 and 3.55 respectively.

The results of the study make it possible to predict, with some certainty, local and average heat transfer coefficients for liquid metals flowing turbulently through eccentric annuli under the above boundary conditions.

1. Introduction

The purpose of the present paper is to present the results of an analytical study on heat transfer rates to liquid metals flowing in eccentric annuli. The paper is the eighth thus far in a published series [1,2, 3,4,5,6,7], originating at the Brookhaven National Laboratory, on the general subject of heat transfer to liquid metals flowing through annuli.

The scope of the study is indicated by the following conditions and ranges of variables which were covered:

a. Prandtl number, 0.00735

b. Peclet number, 368 to 8000

c. Reynolds number, 5×10^4 to 10^6

d. Ratio of outer to inner radius, R, 1.0 to 4.0

e. Eccentricity, e, 0 to 0.70

f. Heat transfer from inner wall only

g. Uniform heat flux

h. Fully developed velocity and temperature profiles

The following assumptions were made:

a. Physical properties of liquid metal were independent of transverse temperature variation.

b. Axial conduction of heat was negligible.

c. Effects from secondary flow patterns were negligible.

These three assumptions are standard in analytical heat transfer studies for turbulent flow of liquid metals, particularly for the heat transfer conditions listed above. The results of the present study are summarized in the form of local normalized coefficients, $h/\bar{h}$, expressed as a function of θ, e, $\bar{\psi}$Pe, and R; and average Nusselt numbers expressed as a function of e, $\bar{\psi}$Pe, and R.

The calculations were all carried out for a single Prandtl number, which is that for sodium at 400°F; but since Prandtl number is not an important variable for liquid metals, it can be safely assumed that the results are applicable for any Prandtl number in the range 0.005 to 0.03, when they are presented in the form of Nusselt numbers as functions of Peclet number.

It is well known that, for heat transfer to liquid metals in turbulent, channel flow, the Nusselt number can be adequately expressed as a function of the product $\bar{\psi}$Pe. Therefore, in the present study, $\bar{\psi}$ was always taken as unity, but the results are expressed in terms of $\bar{\psi}$Pe, which was therefore always numerically equal to the Peclet number.

Geometrical asymmetry has been known to have a deleterious effect on average heat transfer rates to or from liquid metals flowing in

certain types of channels. The reason this effect is more pronounced for liquid metals than for ordinary fluids, is that, in the former, the temperature drop from wall to channel center (in the case of heating) is not restricted to the region very close to the wall, as in the latter. In the present case, local coefficients in the region of lesser clearance are depressed more than those in the region of greater clearance are increased, the result being that the average heat transfer coefficient always falls below that for the concentric case.

The first investigators to observe the effect of asymmetry on liquid-metal heat transfer in annuli were Hall and Jenkins [8,9]. In their experimental study of countercurrent sodium flow in double annuli, they found that there were appreciable variations in temperature around the circumference of the separating pipe, and they attributed this to slight eccentricity of the annuli.

Later, Jenkins and McKee [10], in measuring heat transfer rates between NaK streams flowing through adjacent annuli formed by three pipes, the first inside the second and the second inside the third, found that for an eccentricity of 0.16, the average coefficient for heat transfer from the outer wall of inner annulus was about 25% below that for the concentric case.

In 1960, Subbotin et al. [11], in reporting on a study of heat transfer from the outer wall of an annulus to turbulently flowing mercury, stated that a slight departure from concentricity markedly lowered the average heat transfer coefficient.

Prior to the present study, there were two studies carried out at Brookhaven which shed light on the effects of geometrical asymmetry on liquid-metal heat transfer. In 1961, Friedland et al. [12] reported that, in an experimental study of heat transfer to turbulent flow of mercury through an unbaffled rod bundle, bowing of the rods were thought to be responsible for reductions as high as 50% in the average heat transfer coefficient. And in 1963, Snyder [4] analyzed slug-flow liquid-metal heat transfer in an eccentric annulus under the following conditions: heat transfer from the inner wall only, no circumferential variation of inner wall temperature, no axial variation in heat flux, and fully-established temperature profiles. For an R ratio of 1.94, he found the average Nusselt number to decrease by about 11 and 24% as the eccentricity increased from 0 to 0.20, and from 0 to 0.40, respectively.

2. Calculation Methods and Procedures

In order to calculate either local or average heat transfer coefficients in noncircular channels, one must first obtain velocity and

temperature grids. The first step in calculating the former is to determine the friction factor, and then the fully-developed pressure gradient along the channel axis.

Friction Factor and Pressure Drop

For concentric annuli, the friction factor, f_o, was computed from f_2 values given by Rothfus, Walker, and Whan [13]. These authors have presented the results of a very thorough and comprehensive experimental and analytical study on pressure drop and velocity profiles for turbulent flow in concentric annuli.

For eccentric annuli, the friction factor, f, is not only a function of the Reynolds number, but also of the degree of eccentricity, and possibly of the radius ratio, R. Regarding the last factor, there are insufficient data available to determine its influence, but it is believed to be very slight. The present authors assumed, therefore, as Diskind [14] did earlier, that the ratio f/f_o is independent of both Reynolds number and radius ratio. Figure 1 shows a plot of f/f_o vs. e, based upon the theoretical correlation of Diskind and the single experimental result of Diskind and Stein [15] for an R value of 1.5. The curve in this figure was used to determine all values of f in the present study.

The pressure drop in an eccentric annulus is given by the well known Poiseulle equation

$$\frac{\Delta P}{L} = \frac{2fv_a^2\rho}{g_o D_e} \tag{1}$$

Velocity Distribution

The velocity distribution in an eccentric annulus was determined by an iterative semigraphical method similar to that used by Deissler and Taylor [16]. However, the present method differed in two important respects: (a) the local velocities were determined along the actual (curved) velocity gradient lines, and (b) the method of determining the local velocities was based upon a velocity-profile correlation [13] for annuli.

The velocity-profile correlations of Rothfus, Walker, and Whan [13] were used, but they were first converted to u^+ vs. y^+ curves. These curves depend upon Reynolds number, radius ratio, and whether the local velocity is being determined on the inside or outside of the radius of maximum velocity. A large number of u^+ vs. y^+ curves were therefore necessary, typical sets of which are shown in Figures 2 and 3.

The following procedure was used to determine the velocity distribution in the flow channel of an eccentric annulus. Conditions of symmetry made it necessary to consider only one half the total flow area.

1. The semicircumference of the inner wall is divided into eight equal lengths. These are numbered from 1 to 8, starting from the point

of maximum separation of the two walls (see Figure 4). Radial lines are then drawn from the center of the inner circle to the circumference of the outer circle, dividing the flow channel into 8 sections.

2. The location of the intersection of the maximum-velocity line and the middle radial dividing line of each section is then determined from the equation

$$(r'_m)^2 = \frac{(r''_2)^2 - r_1^2}{\ln(r''_2/r_1)^2} \qquad (2)$$

where

r'_m = radial distance from center of inner circle to maximum-velocity line,

r_1 = radius of inner circle, and

r''_2 = radial distance from center of inner circle to circumference of outer circle.

This equation is analogous to the equation for laminar flow in a concentric annulus and is also a close approximation for turbulent flow.

From the eight points so determined, the location of the maximum velocity line is tentatively located.

3. The next step is to draw tentative velocity gradient lines bounding the eight flow sections. They are meant to be perpendicular to lines

of constant velocity and therefore are perpendicular to the annulus walls and tangent to the maximum velocity line. These lines intersect the inner and outer circles at the points where the seven radial dividing lines cross the walls (see Figure 4).

4. We are now ready to calculate constant-velocity lines, the first step of which is to compute the shear stress at each wall for each of the eight sections. There are, of course, no shear stresses along the velocity gradient lines. Section 2 will be used for illustrative purposes and is represented in Figure 5. In this section, the shear stess along the inner wall is

$$\tau_{2,1} = (\Delta P/L) \frac{A_{2,1}}{s_{2,1}} \tag{3}$$

and along the outer wall

$$\tau_{2,2} = (\Delta P/L) \frac{A_{2,2}}{s_{2,2}} \tag{4}$$

In the figure, $s_{2,1}$ and $s_{2,2}$ are the circumferential boundary lines for Section 2 at the inner and outer walls, respectively; $A_{2,1}$ is the cross-sectional flow area in Section 2 inside the maximum-velocity line; $A_{2,2}$ is the cross-sectional flow area outside the maximum-velocity line.

In Section 2, dashed constant-velocity gradient lines are drawn from the midpoints of $s_{2,1}$ and $s_{2,2}$ dividing the two subsections in half. These

dashed lines meet at a common point on the maximum-velocity line. Then, using u^+ vs. y^+ plots such as those shown in Figure 2, the distance $y_{2,1}$ along the dotted line from the inner wall, for an arbitrarily chosen linear velocity, is determined. Other $y_{2,1}$ values for other velocities are then determined. A similar procedure is followed in getting $y_{2,2}$ values for arbitrarily chosen velocities in the outer portion of Section 2.

In using the modified Rothfus u^+ vs. y^+ plots, it was decided to use three different R values for each of the eight sections, R_1 for the region near the inner wall, R_2 for the region near the outer wall, and R_a for the middle region. These are given by the equations

$$R_1 = r'_2/r_1 \tag{5}$$

$$R_2 = r_2/r'_1 \tag{6}$$

$$R_a = \tfrac{1}{2}(R_1 + R_2) \tag{7}$$

where r'_1 and r'_2 are defined from the equations

$$(r_{m,2})^2 = (r_2 - \Delta y_2)^2 = \frac{r_2^2 - (r'_1)^2}{\ln(r_2/r'_1)^2} \tag{8}$$

$$(r_{m,1})^2 = (r_1 + \Delta y_1)^2 = \frac{(r'_2)^2 - r_1^2}{\ln(r'_2/r_1)^2} \tag{9}$$

In the last two equations, Δy_1 and Δy_2 are the actual lengths of the curved velocity-gradient lines drawn through the middle of the sections, and mentioned above.

By connecting up the points, for a given local velocity, in all eight sections, a set of constant velocity lines is obtained. With these, a second set of velocity-gradient lines is drawn, perpendicular to these constant velocity lines. The process is then repeated and a new set of constant-velocity lines is determined. This time, the maximum-velocity line is relocated, if necessary, to be consistent with constant velocity lines. A third set of velocity-gradient lines is then drawn, and if they are sufficiently different from the second set, the whole process is repeated again, but this was often found unnecessary. In general, it was found that the greater the eccentricity and the radius ratio, the greater the number of iterations needed.

A typical velocity grid is shown in Figure 6. The average linear velocity calculated from the local velocity lines was found to agree with the original average velocity to within ± 2%.

Eddy Conductivities

In order to calculate the temperature distribution in a flow channel, it is necessary to know how the total effective conductivity, k_{eff}, the sum

of the molecular and eddy conductivities, varies throughout the cross-sectional area. The latter is calculated from the equation

$$k_e = C_p \mu_e \tag{10}$$

which is based upon the condition that the eddy diffusivities of heat and momentum transfer are equal.

The eddy viscosity, μ_e, in the present study was calculated from the standard equation

$$\tau g_o = [\mu + \mu_e] \frac{dv}{dy} \tag{11}$$

where v is the local velocity at distance y from the wall, along the middle, curved, velocity-gradient line in each of the eight sections. The shear stress, τ, at the same point is calculated from the equation

$$\tau = \frac{\Delta P}{L s_\tau} \int_y^{y_m} s\,dy \tag{12}$$

where s_τ is the width of the section, taken perpendicular to the middle velocity-gradient line, at the point where τ is evaluated. The slopes, dv/dy, in Eq. (11) were determined graphically to within a demonstrated precision of ± 3%.

Values of k_{eff} were determined in both the inner and outer portions of each section for arbitrarily chosen values of y along the middle velocity-

gradient lines. From these values, lines of constant k_{eff} were then drawn. A typical k_{eff} grid is shown in Figure 7 where it is seen that there are two maximum-k_{eff} lines, one in the inner and one in the outer portion of the annulus.

Temperature Distribution

In the present study, temperature distributions, including peripheral wall temperature variation, were calculated by two different methods.

In the first, the energy-balance equation

$$\frac{\partial(k_{eff}\frac{\partial t}{\partial x})}{\partial x} + \frac{\partial(k_{eff}\frac{\partial t}{\partial y})}{\partial y} = \rho C_p v \frac{\partial t}{\partial z} \qquad (13)$$

was numerically integrated and solved by a relaxation method with the aid of an IBM 7094 digital computer. The boundary conditions are: (a) the normal temperature derivatives are constant along the inner wall and equal to q/k, and (b) the normal temperature derivatives are zero along the outer wall. The difference equations were set up in polar coordinates and the relaxation was performed for one radius at a time.

A computer program was worked out to solve Eq. (13); however, it required about 10 hours of computer time for each case, and the cost was therefore prohibitive. Consequently, only one case was solved by this method. All the others were solved by a method which was partly

graphical, and which required only a very small fraction of the computer time required by the numerical method.

In the second method, the procedure was as follows:

1. The circumference of the inner semicircle was divided into eight equal segments as before; and then, from these, by an iteration process, the total flow area was divided into eight sections such that, for each, the following equation was obeyed:

$$\int_0^{y_n} vsdy = \frac{v_a \pi [r_2^2 - r_1^2]}{16} \tag{14}$$

The lines separating the various sections are heat-flow lines and, as such, must be perpendicular to the inner wall and tangent to the outer wall (see Figure 8). Since the shape of the velocity profiles are practically independent of Reynolds number, the heat flow lines in this figure are independent of flow rate, and therefore Peclet number. Starting at the midpoints of the inner wall segments, eight additional heat flow lines were drawn through the middle of each section. These are shown as dashed lines in the figure. In Eq. (14), v is the local velocity and s is the width of the section (drawn pependicular to the middle heat flow line), both at the distance y from the inner wall, measured along the middle, curved heat flow line.

Eq. (14) is a consequence of the condition of uniform heat flux, i.e., since the heat transferred from each of the eight inner-wall sub-areas is the same, then the heat transported away by the liquid metal in each of the eight associated cross-sectional sub-areas must also be the same.

2. The next step is to determine the temperature variation along each of the eight middle heat-flow lines. For this, a heat flux of 100,000 $Btu/(hr)(ft)^2$ was arbitrarily chosen, and the temperature at point a in Figure 8 was arbitrarily taken as 400^0F.

Considering Section 1, the temperature drop between point a and some other point at a distance y from a along the middle heat-flow line is given by the identity

$$\Delta t = -\int_0^y \frac{\partial t}{\partial y}\, dy \tag{15}$$

where the temperature gradient at y, $\partial t/\partial y$, is obtained from the heat balance

$$-k_{eff}\, s\, \frac{\partial t}{\partial y} = C_p \rho\, \frac{dt}{dz} \int_y^{y_1} v s dy \tag{16}$$

The left side of this equation represents the heat transferred across

the line s at y, and the right side represents the heat transported away by the fluid flowing in the cross-sectional area beyond the line s. Substituting Eq. (16) in (15), finally gives

$$\Delta t = C_p \rho \frac{dt}{dz} \int_0^y \frac{\int_y^{y_1} svdy}{k_{eff}\, s}\, dy \tag{17}$$

Using this equation, values of Δt are then calculated for various values of y. The results are smoothed by drawing Δt vs. y curves. The process is then repeated for the other seven sections.

3. The 400°F isotherm is then drawn from point a, perpendicular to the heat flow lines, as shown in Figure 8. With this as a "bench mark," and using the Δt vs. y plots mentioned above, a family of isotherm lines is then drawn throughout the whole half-annulus cross section. These isotherms are tangent to the inner wall and perpendicular to the outer wall. From them, the bulk temperature in Section 1 is obtained by the equation

$$t_{b_1} = \frac{\int_0^{y_1} tvsdy}{\int_0^{y_1} vsdy} \tag{18}$$

and similarly for the other seven sections. The over-all bulk temperature for the annulus is then given by

$$t_b = \frac{t_{b_1} + t_{b_2} + \ldots + t_{b_8}}{8} \tag{19}$$

Finally, the local heat transfer coefficient, h, for Section 1 is given by

$$h_1 = \frac{q}{t_{w_1} - t_b} \tag{20}$$

and similarly for the other seven sections. And the average heat transfer coefficient, $\bar{h}$, for the whole annulus is given by

$$\bar{h} = \frac{q}{\bar{t}_w - t_b} \tag{21}$$

3. Results

Surface Temperature Variation

It was found that eccentricity produced a surprisingly large amount of temperature variation around the circumferences of both walls. The variation around the inner wall is of greater practical interest, and the results for this are shown in Figure 9, where the variations are expressed as the ratio $\left(t_w\right]_{180^o} - t_w]_{0^o}\right)/(\bar{t}_w - t_b)$. This ratio is independent of the heat flux, as long as it is uniform. The lower the radius ratio, and the

greater the eccentricity, the greater will be the relative temperature variation around the wall surface. This relative variation, as expressed by the above ratio, is essentially independent of Peclet number. It is seen that under certain circumstances the circumferential temperature variation can far exceed the difference between the average surface temperature and bulk temperature. The reason for the relatively large temperature variation is quickly apparent from inspection of Figure 8, where it is seen that the heat from that portion of the inner wall nearest the outer wall is transferred over a much longer cross-sectional area (Section 8), than of heat transferred from that portion of the inner wall farther from the outer wall (Section 1). The effect of eccentricity on temperature variation around the inner wall, for the worst case studied, is shown graphically in Figure 10.

Local Coefficients

Since eccentricity causes considerable circumferential variation in the temperature of the inner wall, it follows that there will also be a concomitant variation in the local heat transfer coefficient. At low values of R, the variation can be so great as to give negative coefficients in the region of widest separation between the two walls. This is simply because the surface temperatures in that region are below the over-all

bulk temperature of the metal flowing through the annulus. Figure 11 shows some typical profiles for this case. The local coefficients are normalized by dividing them by the average coefficient. The reader is reminded that, since $\bar{h} \neq \frac{1}{\pi}\int_0^{\pi} h d\theta$ but is given by Eq. (21), the algebraic sum of the areas between $h/\bar{h} = 1$ and the curves does not approach zero.

The curves shown in Figure 11 should be, for all practical purposes, independent of the Peclet number. The spread in the data points, which of course worsens as the angle of infinite coefficient is approached, is simply due to limitations in calculational precision. The angle of infinite coefficient is obviously the point on the inner wall where the temperature is equal to the bulk temperature of the metal flowing through the annulus at that same axial location.

Figure 12 shows a set of coefficient profiles for two different values of R and two different eccentricities, where the local coefficients are always positive. Here, as in the previous figure, the areas between the curves and the ordinate line of unity should not add to zero.

Tables I and II summarize, in normalized form, all the local heat transfer coefficient results obtained under the study. Theoretically, Peclet number should have a negligibly small effect on the normalized coefficients. The differences shown in the tables simply reflect the

degree of precision for the long and involved method of calculation.

Average Coefficients and Nusselt Numbers

The average heat transfer coefficients and Nusselt numbers obtained under the study are shown in Table III. The values for zero eccentricity given there were calculated from the recent correlation of Dwyer [17]

$$Nu_0 = \alpha + \beta(\bar{\psi}Pe)^{\gamma} \tag{22}$$

where

$$\alpha = 4.58 + 0.742R$$

$$\beta = 0.0290 - 0.00414R + 0.000364R^2$$

$$\gamma = 0.725R^{0.091}$$

This correlation is also based upon the velocity-profile correlation of Rothfus et al. and upon ϵ_M profile shape a shown in Figure 17. It should, therefore, give Nusselt values consistent with those calculated in the present study for eccentric annuli.

Many of the average Nusselt results are also shown graphically in Figures 13-16. From the curves in each of these figures, we see that, other things being equal, increase in eccentricity always decreases the Nusselt number. In Figure 14 we see that, at low eccentricities, the

greater the radius ratio, the less the effect of eccentricity; while at high eccentricities, the greater the radius ratio, the greater the effect of eccentricity. In Figures 15 and 16 we see that the effect of eccentricity is independent of Peclet number. Finally, in all four figures we see that the effect of eccentricity on the Nusselt number if great indeed, at practically all values of R and Peclet number.

4. Discussion of Results

The first question to be asked is: how precise are the calculated results? An estimate of this can be obtained from the fact that for the case of R = 1.5, e = 0.70, and $\bar{\psi}Pe = 368$, the average heat transfer coefficient was obtained by the two methods described in Section 2. The all-machine solution of Eq. (13) gave a value of 677 Btu/(hr)(ft)^2($^\circ$F), while the combination graphical-machine method gave 656, a difference of about 3%. Another estimate of the precision is given by the scatter of the calculated points on the various graphs, which indicates a precision of within $\pm 5\%$.

The next question to be asked is: how accurate are the calculated results? This is more difficult to answer. For one thing, there are no experimental results available for comparison. It is well to remember that the boundary conditions for this study, i.e., uniform heat flux from

the inner wall of an eccentric annulus, cannot be fully obtained in practice. The conditions can only be met when either the thickness of the wall approaches zero, or the thermal conductivity of the wall approaches zero, or both. In any real case, the circumferential temperature variation caused by the eccentricity produces circumferential heat flow in the wall, causing departure from the condition of uniform flux and thereby mitigating the effect of eccentricity on the variation of wall temperature, the variation of the local heat transfer coefficient, and the value of the average heat transfer coefficient.

The boundary conditions chosen in the present study therefore represent upper limits to the effects of eccentricity on wall temperature, the local coefficient, and the average coefficient, which under certain conditions may be approached but never attained. The next step is to consider the effects of the thickness and conductivity of the wall on the thermal behavior of eccentric annuli. However, all of the general conclusions reached in the present study are equally applicable to the case where there is circumferential heat flow in the inner wall.

In their analytical study for air, Deissler and Taylor [16] predicted a 73% decrease in the average Nusselt number as the eccentricity was

increased from 0 to 80% in an annulus having an R value of 3.5 and heat transfer from the inner wall only. By inspection of Figure 14, the predicted decrease in the Nusselt number for liquid metals under the same conditions is about 78%. The present authors would agree that the decrease should be greater for liquid metals, but feel that these two predictions, if anything, are a bit too close.

In calculating ϵ_H from ϵ_M, one is never completely certain of the shape of the ϵ_M profile in the region of maximum velocity. In the present study, the ϵ_M profile curves had the shape a in Figure 17. There is good reason to believe that they should have the general shape b, with the curve crossing the radius of maximum velocity at an ϵ_M value about 75% of its maximum [6,7]. For heat transfer in pipes, the shape of the ϵ_M curve has an insignificant effect on the coefficient; but for annuli, the effect has been estimated to be about 1% at $\bar{\psi}Pe = 10^2$, 5% at $\bar{\psi}Pe = 10^3$, and 10% at $\bar{\psi}Pe = 10^4$ [18]. The reason the effect is much greater for annuli (with heat transfer from the inner wall only) is that there is an appreciable radial temperature gradient in the transverse region of maximum velocity. It is logical to assume that the shape of the ϵ_M profile curves would have a comparable effect in the case of eccentric annuli. Therefore, it is recommended that the Nusselt numbers given in this

paper be increased, in accordance with the above percentages, if they are to be used in design calculations.

In using the results given in this paper to estimate heat transfer coefficients, one needs to evaluate the $\bar{\psi}$Pe product, and therefore $\bar{\psi}$. There are a number of correlations available for estimating $\bar{\psi}$, but the present authors recommend that recently proposed by Dwyer [19], for simplicity and adequate accuracy.

5. Acknowledgments

The authors gratefully acknowledge the invaluable assistance of the following Brookhaven people: John R. Cannon, David A. Beaucage, and Nechemiah Reiss of the Applied Mathematics Department for developing the computer program for the all-machine calculational method; Irene Nicodemus of the same department for her assistance with the computer programming for the semigraphical method; and Peter Hlavac, Donald Siefkes, Stephen Gordon, and P. S. Tu of the Nuclear Engineering Department for their assistance with the calculations at various times.

6. Nomenclature

$A_{2,1}$ = Cross-sectional flow area in Section 2 inside the maximum-velocity line, ft^2

$A_{2,2}$ = Cross-sectional flow area in Section 2 outside the maximum-velocity line, ft^2

C_p = Specific heat, Btu/(lb-mass)(^{0}F)

D_e = Equivalent diameter of the annulus

$$= \frac{4(\text{cross-sectional flow area})}{\text{wetted perimeter}}, \text{ ft}$$

d = Distance between the centers of the two circles forming the annulus, ft

e = Eccentricity = $d/(r_2-r_1)$, dimensionless

f = Fanning friction factor for an eccentric annulus, dimensionless

f_2 = Fanning friction factor for the outer portion of a concentric annulus (between the maximum velocity line and the outer wall), dimensionless

f_o = Fanning friction factor for a concentric annulus, dimensionless

g_o = Conversion factor, (lb-mass)(ft)/(lb-force)$(hr)^2$

h = Local heat transfer coefficient, Btu/(hr)$(ft)^2(^0F)$

h_1 = Local heat transfer coefficient for Section 1, Btu/(hr)$(ft)^2(^0F)$

$\bar{h}$ = Average heat transfer coefficient for the whole annulus, Btu/(hr)$(ft)^2(^0F)$

k = Molecular thermal conductivity, Btu/(hr)(ft)($^{\circ}$F)

k_e = Eddy thermal conductivity, Btu/(hr)(ft)($^{\circ}$F)

k_{eff} = $k + k_e$ = Effective thermal conductivity, Btu/(hr)(ft)($^{\circ}$F)

L = Length of annular channel, ft

Nu = $(hD_e)/k$ = Nusselt number, dimensionless

Nu_o = Nusselt number for a concentric annulus, dimensionless

n = 1,2,. . .,8 = Section number, dimensionless

ΔP = Pressure drop over distance L, lb-force/ft^2

Pe = $D_e v_a \rho C_p/k$ = Peclet number, dimensionless

Pr = $C_p \mu/k$ = Prandtl number, dimensionless

q = Heat flux, Btu/(hr)(ft)^2

R = r_2/r_1 = Radius ratio, dimensionless

R_1 = r'_2/r_1 = Radius ratio, dimensionless

R_2 = r_2/r'_1 = Radius ratio, dimensionless

R_a = $\frac{1}{2}(R_1 + R_2)$ = Average radius ratio, dimensionless

Re = $D_e v_a \rho/\mu$ = Reynolds number, dimensionless

r_1 = Inner radius of an annulus, ft

r_2 = Outer radius of an annulus, ft

r'_1 = Fictive inner radius of an annulus, defined by Eq. (8), ft

r'_2 = Fictive outer radius of an annulus, defined by Eq. (9), ft

r''_2 = Radial distance from center of inner circle to circumference of outer circle, ft

r_m = Radius of maximum fluid velocity in a concentric annulus, ft

r'_m = Radial distance from center of inner circle to maximum-velocity line, ft

$r_{m,1}$ = Radius of maximum fluid velocity, defined by Eq. (9), ft

$r_{m,2}$ = Radius of maximum fluid velocity, defined by Eq. (8), ft

$s_{2,2}$ = Circumferential boundary line for Section 2 at the outer wall, ft

$s_{2,1}$ = Circumferential boundary line for Section 2 at the inner wall, ft

s = Width of the section, taken perpendicular to the middle velocity-gradient line and/or the middle heat flow line, at the curved distance y from the wall, ft

s_τ = s at the point where τ is evaluated, ft

t = Temperature of the fluid at y, or at (x,y,z), °F

t_b = Bulk temperature of the fluid, °F

$t_{b_1}, t_{b_2}, \ldots, t_{b_8}$ = Fluid bulk temperature of Section 1, 2, ..., and 8, °F

t_{w_1} = Inner wall surface temperature of Section 1, °F

$\bar{t}_w$ = Average inner wall surface temperature of an annulus, °F

$t_{w]_\theta}$ = Inner wall surface temperature at an angle θ of an annulus, °F

Δt = Temperature drop from the inner wall to y of the fluid in an annulus, °F

u^+ = Velocity parameter, dimensionless

u_1^+ = Velocity parameter for the inner portion of an annulus, dimensionless

u_2^+ = Velocity parameter for the outer portion of an annulus, dimensionless

v = Linear velocity of fluid at y or at (x,y,z), ft/sec

v_a = Average linear velocity of the fluid, ft/sec

x,y,z = Cartesian coordinates, defined only for Eq. (13)

y = Normal curved distance from the wall, or vertical Cartesian coordinate, ft

y^+ = Normal distance parameter, dimensionless

y_m = Value of y at the maximum velocity, ft

y_n = Value of y from the inner wall to the outer wall of Section n, ft

y_1 = Value of y_n for n = 1, ft

$y_{2,1}$ = Normal curved distance along the middle velocity gradient line from the inner wall of Section 2, ft

$y_{2,2}$ = Normal curved distance along the middle velocity gradient line from the outer wall of Section 2, ft

y_1^+ = Wall distance parameter for the inner portion of an annulus, dimensionless

y_2^+ = Wall distance parameter for the outer portion of an annulus, dimensionless

Δy_1 = Length of the middle, curved velocity-gradient line from the inner wall to the maximum velocity line, ft

Δy_2 = Length of the middle, curved velocity-gradient line from the outer wall to the maximum velocity line, ft

z = Axial distance along the annulus, or Cartesian coordinate, ft

Greek Letters

α,β,γ = Constants defined by Eq. (22), dimensionless

ϵ_H = $k_e/\rho C_p$ = Eddy diffusivity of heat transfer, ft^2/hr

ϵ_M = μ_e/ρ = Eddy diffusivity of momentum transfer, ft^2/hr

θ = Clockwise angle made with the center of inner circle, radian

μ = Fluid dynamic viscosity, (lb-mass)/(ft)(hr)

μ_e = Fluid eddy viscosity, (lb-mass)/(ft)(hr)

ρ = Fluid density, $(lb\text{-mass})/ft^3$

τ = Shear stress in the fluid at a distance y from the wall, $(lb\text{-force})/ft^2$

$\tau_{2,1}$ = Shear stress pertaining to the inner wall of Section 2, $(lb\text{-force})/ft^2$

$\tau_{2,2}$ = Shear stress pertaining to the outer wall of Section 2, (lb-force)/ft^2

$\bar{\psi}$ = Average effective value of ψ (= ϵ_H/ϵ_M), dimensionless

7. References

1. O. E. Dwyer and P. S. Tu, "Unilateral heat transfer to liquid metals flowing in annuli," Nucl. Sci. Eng. 15, 58-68 (1963).
2. O. E. Dwyer, "Equations for bilateral heat transfer to a fluid flowing in a concentric annulus," Nucl. Sci. Eng. 15, 52-7 (1963).
3. O. E. Dwyer, "On the transfer of heat to fluids flowing through pipes, annuli, and parallel plates," Nucl. Sci. Eng. 17, 336-44 (1963).
4. William T. Snyder, "An analysis of slug flow heat transfer in an eccentric annulus," AIChE Journal 9, No. 4, 503-6 (1963).
5. O. E. Dwyer, "Bilateral heat transfer in annuli for slug and laminar flows," Nucl. Sci. Eng. 19, 48-57 (1964).
6. O. E. Dwyer, "Heat transfer to liquid metals flowing turbulently between parallel plates," accepted for publication in Nucl. Sci. Eng.
7. O. E. Dwyer and P. S. Tu, "Bilateral heat transfer to liquid metals flowing turbulently through annuli," accepted for publication in Nucl. Sci. Eng.
8. W. B. Hall and A. E. Jenkins, "Heat transfer experiments with sodium," United Kingdom Atomic Energy Authority, R&DB(W)-8054 (1953).
9. W. B. Hall and A. E. Jenkins, "Heat transfer experiments with sodium and sodium-potassium alloy," J. Nucl. Energy 1, 244-63 (1955).

10. A. E. Jenkins and G. McKee, "Heat transfer experiments with sodium potassium alloy," United Kingdom Atomic Energy Authority, R&DB(W)TN-198 (1955).

11. V. I. Subbotin, P. A. Ushakov and I. P. Sviridenko, "Heat transfer to mercury flowing turbulently in an annulus," Atomnaya Energiya (Atomic Energy USSR) 9, No. 4, 310-2 (1960).

12. A. J. Friedland, O. E. Dwyer, M. W. Maresca and C. F. Bonilla, "Heat transfer to mercury in parallel flow through bundles of circular rods," International Heat Transfer Conference, Part III, p. 526, Boulder, Colorado (1961).

13. R. R. Rothfus, J. E. Walker and G. A. Whan, "Correlation of local velocities in tubes, annuli, and parallel plates," AIChE Journal 4, No. 2, 240-5 (1958).

14. T. Diskind, "Convection heat transfer in noncircular ducts," Columbia University, NYO-9646 (1960).

15. T. Diskind, C. A. Matos and R. P. Stein, "Initial experiments on pressure drop for flow through eccentric annuli," Columbia University, TID-5670 (1959).

16. Robert G. Deissler and Maynard F. Taylor, "Analysis of fully developed turbulent heat transfer and flow in an annulus with various eccentricities," Nat. Adv. Comm. Aero. Technical Note 3451 (1955).

17. O. E. Dwyer, "On the transfer of heat to fluids flowing through pipes, annuli, and parallel plates," BNL 6692 (1963).

18. O. E. Dwyer, "Liquid-metal heat transfer," paper presented at the Third Geneva Conference on Peaceful Uses of Atomic Energy, August 31 - September 9, 1964.

19. O. E. Dwyer, "Eddy transport in liquid-metal heat transfer," AIChE Journal 9, No. 2, 261-8 (1963).

Table I

Circumferential Variation of Normalized Heat Transfer Coefficient Around Inner Wall for R = 1.5

	$h/\bar{h}$									
	$\bar{\psi}Pe = 368$				$\bar{\psi}Pe = 1700$				$\bar{\psi}Pe = 8000$	
θ	e=0.15	e=0.30	e=0.50	e=0.70	e=0.15	e=0.30	e=0.50	e=0.70	e=0.30	e=0.70
11.25	-2.31	-1.10	-1.54	-1.31	-2.35	-1.06	-1.79	-2.78	-1.28	-2.81
33.75	-2.69	-1.35	-1.81	-1.61	-2.94	-1.34	-2.13	-3.47	-1.97	-3.65
56.25	-200.00	-6.06	-5.28	-3.20	640.00	-3.98	-5.00	-6.42	-7.47	-6.88
78.75	1.27	1.52	1.79	1.70	1.27	2.19	2.67	4.02	2.00	8.93
101.25	0.69	0.65	0.71	0.55	0.65	0.76	0.81	1.13	0.79	1.72
123.75	0.51	0.46	0.48	0.28	0.51	0.45	0.47	0.53	0.48	0.60
146.25	0.44	0.38	0.39	0.21	0.46	0.35	0.38	0.37	0.38	0.34
168.75	0.42	0.36	0.36	0.21	0.44	0.32	0.35	0.33	0.34	0.29

Table II

Circumferential Variation of Normalized Heat Transfer Coefficient Around Inner Wall for $\bar{\psi}Pe = 1700$

	$h/\bar{h}$					
	R = 1.5		R = 2.5		R = 4.0	
θ	e=0.30	e=0.70	e=0.30	e=0.70	e=0.30	e=0.70
11.25	-1.06	-2.78	2.03	3.59	1.56	1.75
33.75	-1.34	-3.47	1.89	3.05	1.53	1.67
56.25	-3.98	-6.42	1.70	2.54	1.41	1.57
78.75	2.19	4.02	1.39	1.96	1.18	1.40
101.25	0.76	1.13	0.98	1.12	0.97	1.02
123.75	0.45	0.53	0.73	0.64	0.81	0.75
146.25	0.35	0.37	0.63	0.51	0.72	0.65
168.75	0.32	0.33	0.60	0.48	0.67	0.62

Table III

Calculated Average Heat Transfer Coefficients and Average Nusselt Numbers for Heat Transfer to Liquid Metals Flowing Through Eccentric Annuli

R	e	$\bar{\psi}$Pe	$\bar{h}$	Nu
1.5	0.00	368	8700.0	7.70
		1700	13590.0	12.04
		8000	29490.0	26.11
	0.15	368	4070.9	3.61
		1700	7131.7	6.32
	0.30	368	2634.0	2.34
		1700	4494.9	3.99
		8000	10244.0	9.08
	0.50	368	1207.5	1.07
		1700	1794.8	1.59
	0.70	368	656.5	0.58
		1700	980.5	0.87
		8000	2340.4	2.08
2.5	0.00	1700	8610.0	13.75
	0.30	1700	5475.7	8.74
	0.70	1700	2052.7	3.28
4.0	0.00	1700	7920.0	15.80
	0.30	1700	6524.6	13.01
	0.70	1700	2848.7	5.68

Figure Captions

Figure 1 Effect of degree of eccentricity on friction factor for flow in eccentric annuli. Curve is based on the analytical prediction of Diskind [14] and on the single experimental measurement of Diskind and Stein [15] for an annulus having an R value of 1.5.

Figure 2 Modified Rothfus velocity distributions for the inner portion of an annulus, R = 1.5, symbols represented calculated values.

Figure 3 Modified Rothfus velocity distributions for the outer portion of an annulus, R = 1.5, symbols represented calculated values.

Figure 4 Cross section of eccentric annulus, showing division into sections, and location of tentative maximum-velocity line and tentative velocity-gradient lines. Numbers refer to sections.

Figure 5 Schematic drawing of a typical section of an eccentric annulus showing meaning of symbols. Section 2 is taken as an example.

Figure 6 Velocity distribution for an eccentric annulus. e = 0.30; $Re = 2.3 \times 10^5$; R = 2.5; v_a = 16.38 ft/sec. Numbers on graph represent constant velocity lines, expressed in ft/sec.

Figure 7 Effective thermal conductivity distribution for sodium flowing in an eccentric annulus under fully-developed flow and thermal condition. e = 0.30; Re = 2.3×10^5; Pr = 0.00735; R = 2.5. Numbers on graph represent constant k_{eff} lines, expressed in Btu/(hr)(ft)(°F).

Figure 8 Graph showing heat flow lines and 400°F isotherm for an eccentric annulus with uniform heat flux from inner wall, e = 0.30 and R = 1.5.

Figure 9 Relative circumferential temperature variation around inner wall, Pr = 0.00735.

Figure 10 Relative variation of inner wall surface temperature for uniform heat flux through inner wall. $\bar{\psi}$Pe = 368 and R = 1.5.

Figure 11 Circumferential variation of normalized heat transfer coefficient around inner wall.

Figure 12 Circumferential variation of normalized heat transfer coefficient around inner wall.

Figure 13 Average Nusselt number vs. eccentricity, with radius ratio as the parameter. Inner wall heated only; $\bar{\psi}$Pe = 1700.

Figure 14 Ratio of average Nusselt number to concentric Nusselt number vs. eccentricity.

Figure 15 Average Nusselt number vs. Peclet number, with eccentricity as the parameter. Inner wall heated only; R = 1.5.

Figure 16 Average Nusselt number vs. concentric Nusselt number for R = 1.5 and for different values of e.

Figure 17 Typical ϵ_M and temperature profiles for heat transfer to a liquid metal flowing in an annulus. Curves a and b represent different types of ϵ_M profile curves. r_1, r_2, and r_m represent inner radius, outer radius, and radius of maximum velocity, respectively.

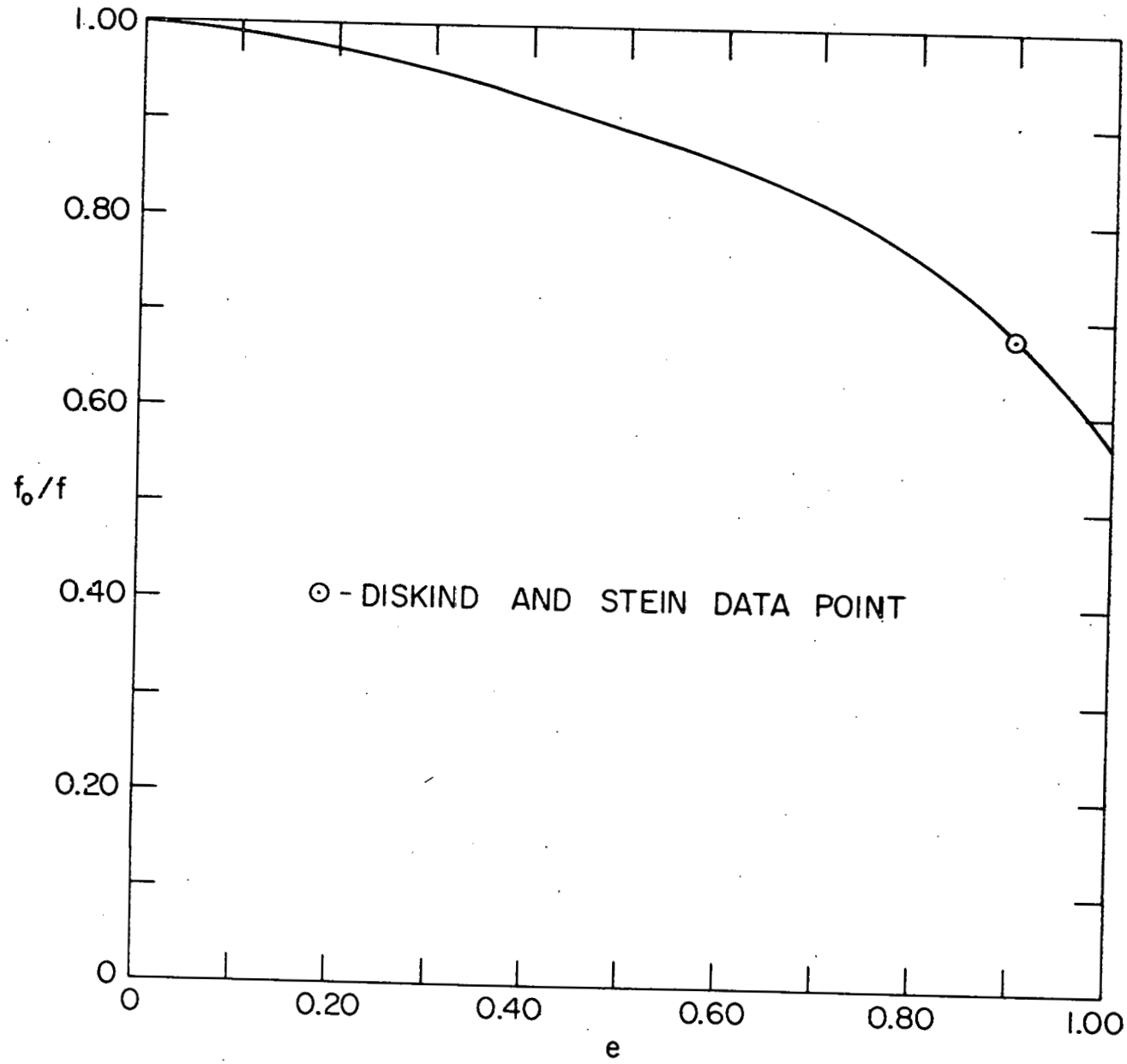

Figure 1 - NUCLEAR SCIENCE & ENGINEERING - Yu and Dwyer

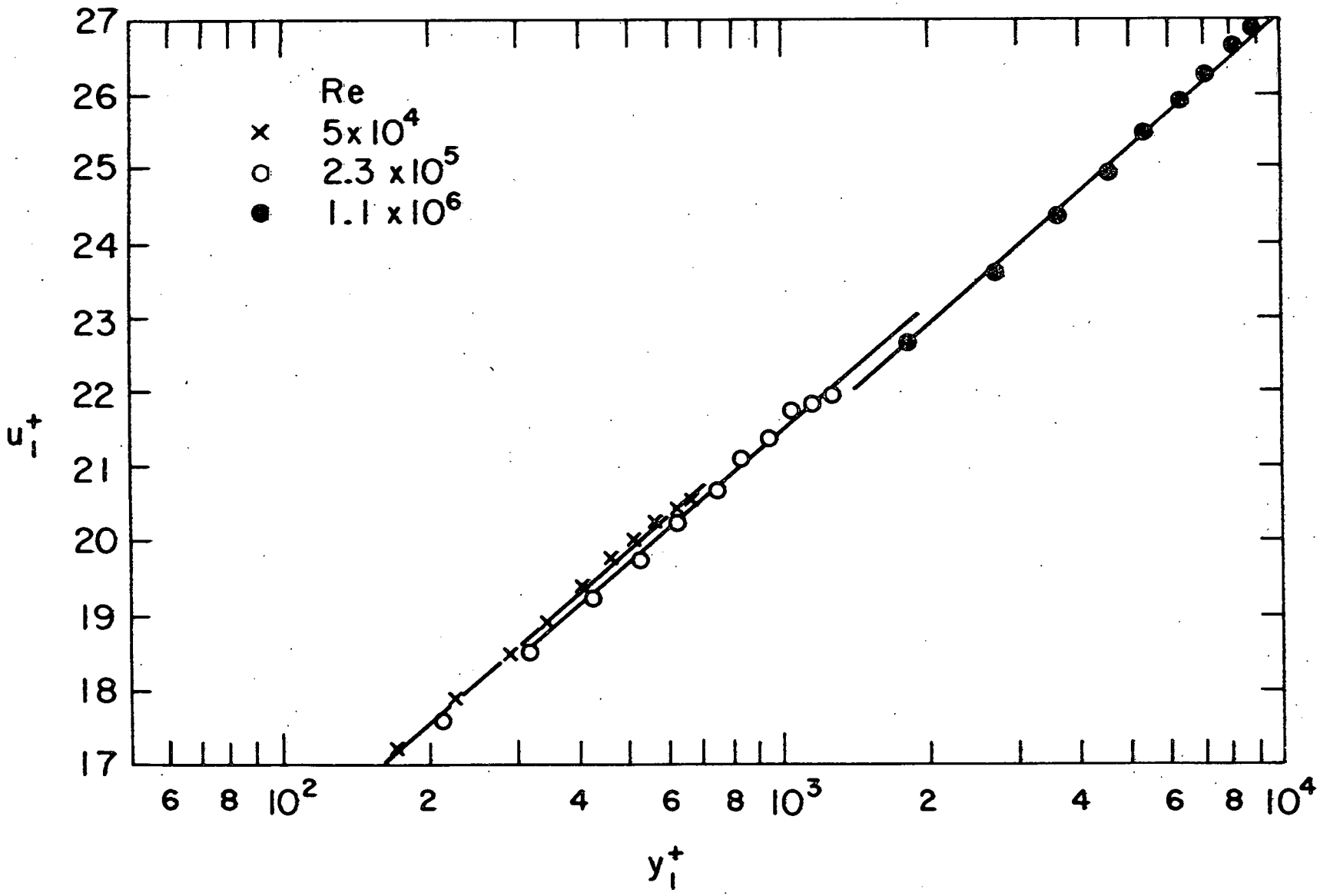

Figure 2 - NUCLEAR SCIENCE & ENGINEERING - Yu and Dwyer

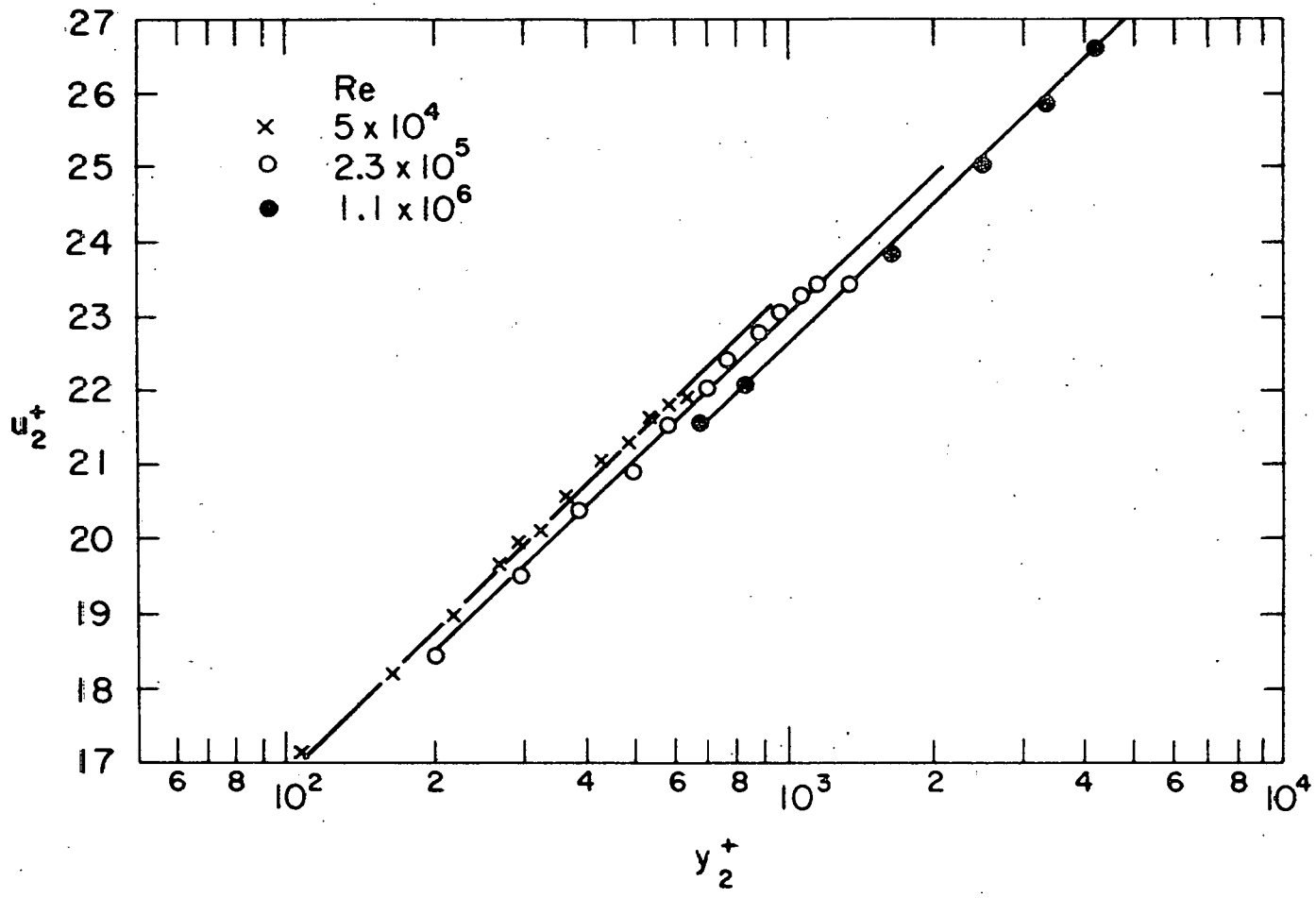

Figure 3 - NUCLEAR SCIENCE & ENGINEERING - Yu and Dwyer

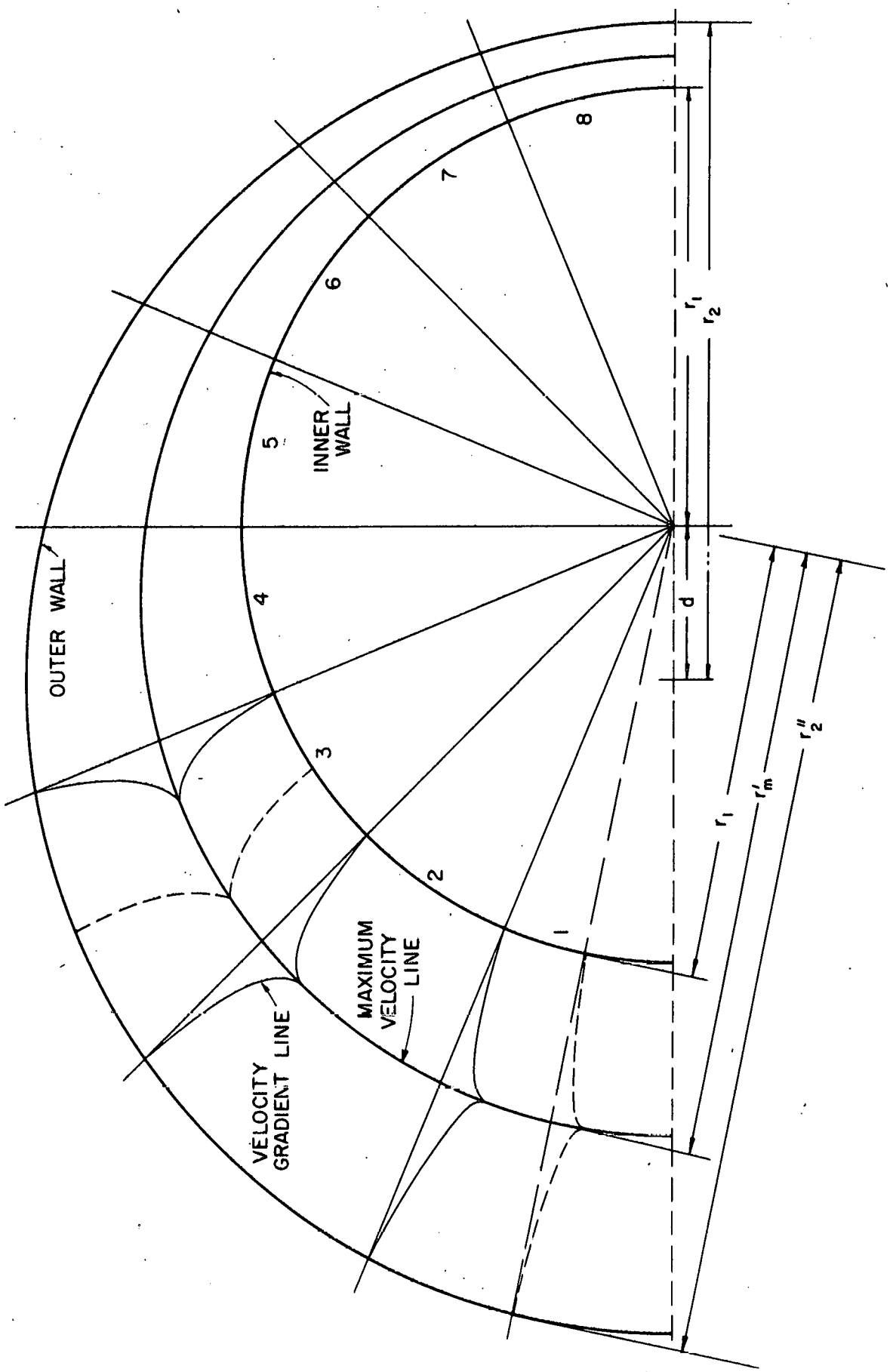

Figure 4 - NUCLEAR SCIENCE & ENGINEERING - Yu and Dwyer

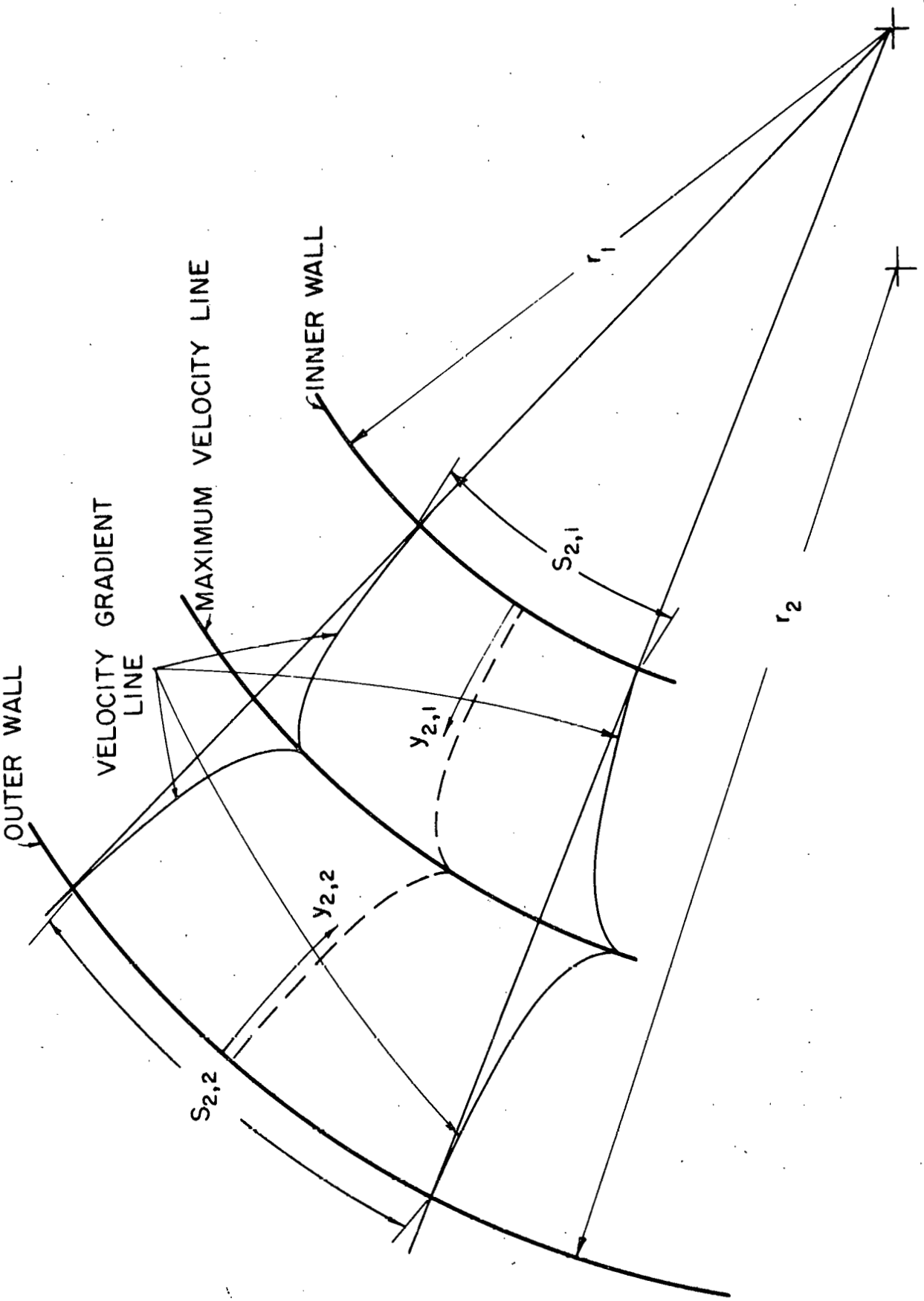

Figure 5 - NUCLEAR SCIENCE & ENGINEERING - Yu and Dwyer

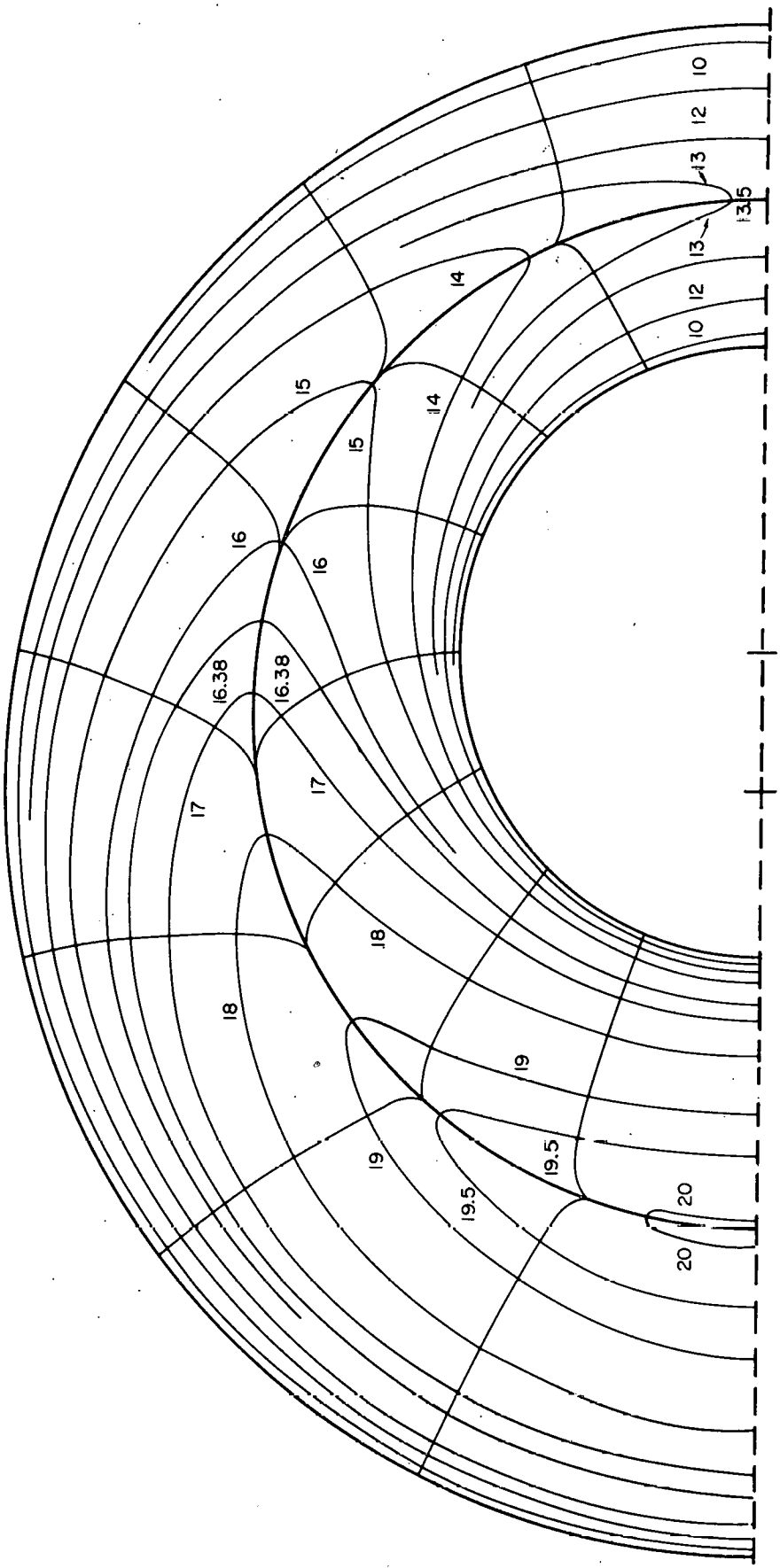

Figure 6 - NUCLEAR SCIENCE & ENGINEERING - Yu and Dwyer

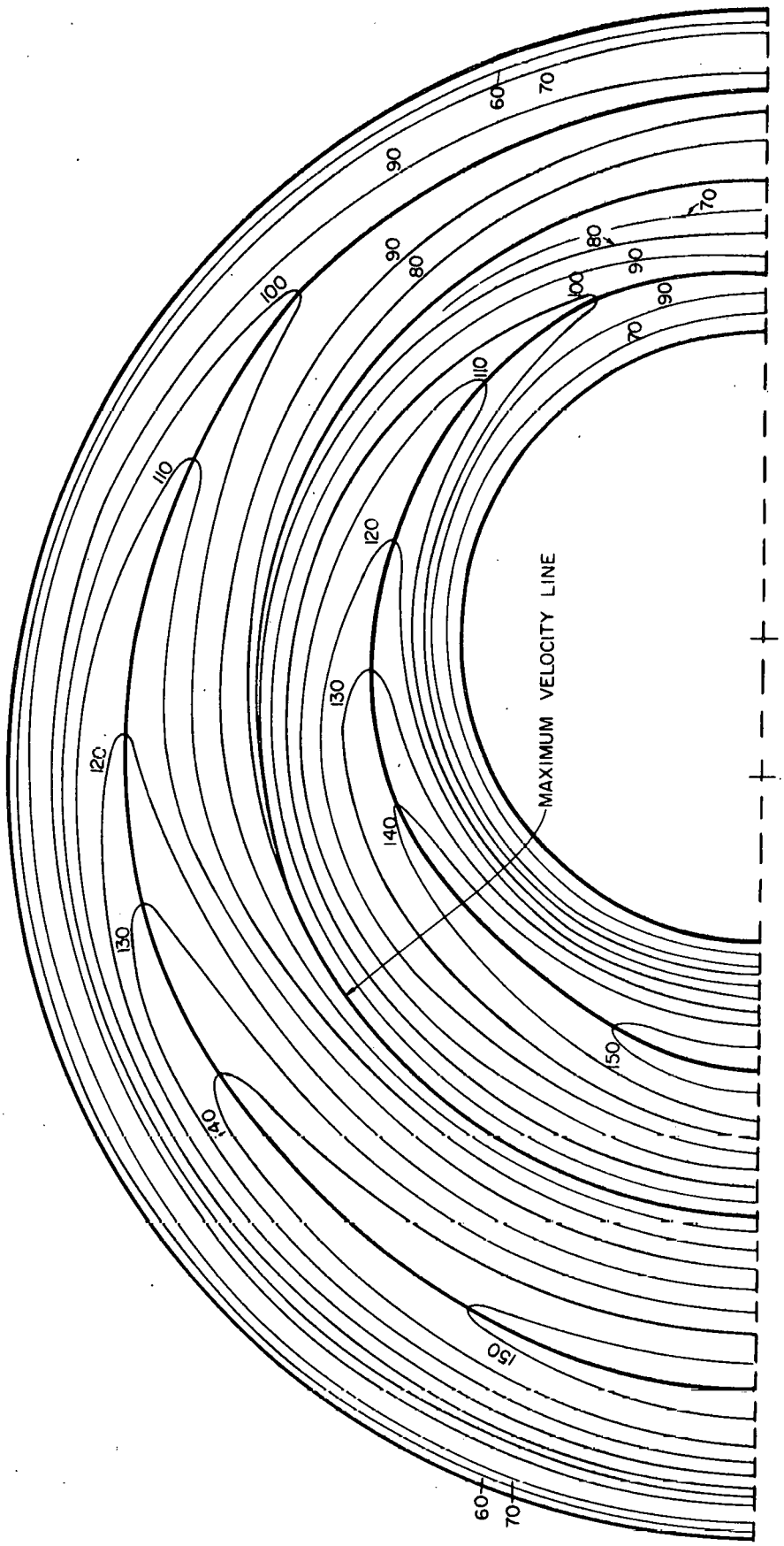

Figure 7 - NUCLEAR SCIENCE & ENGINEERING - Yu and Dwyer

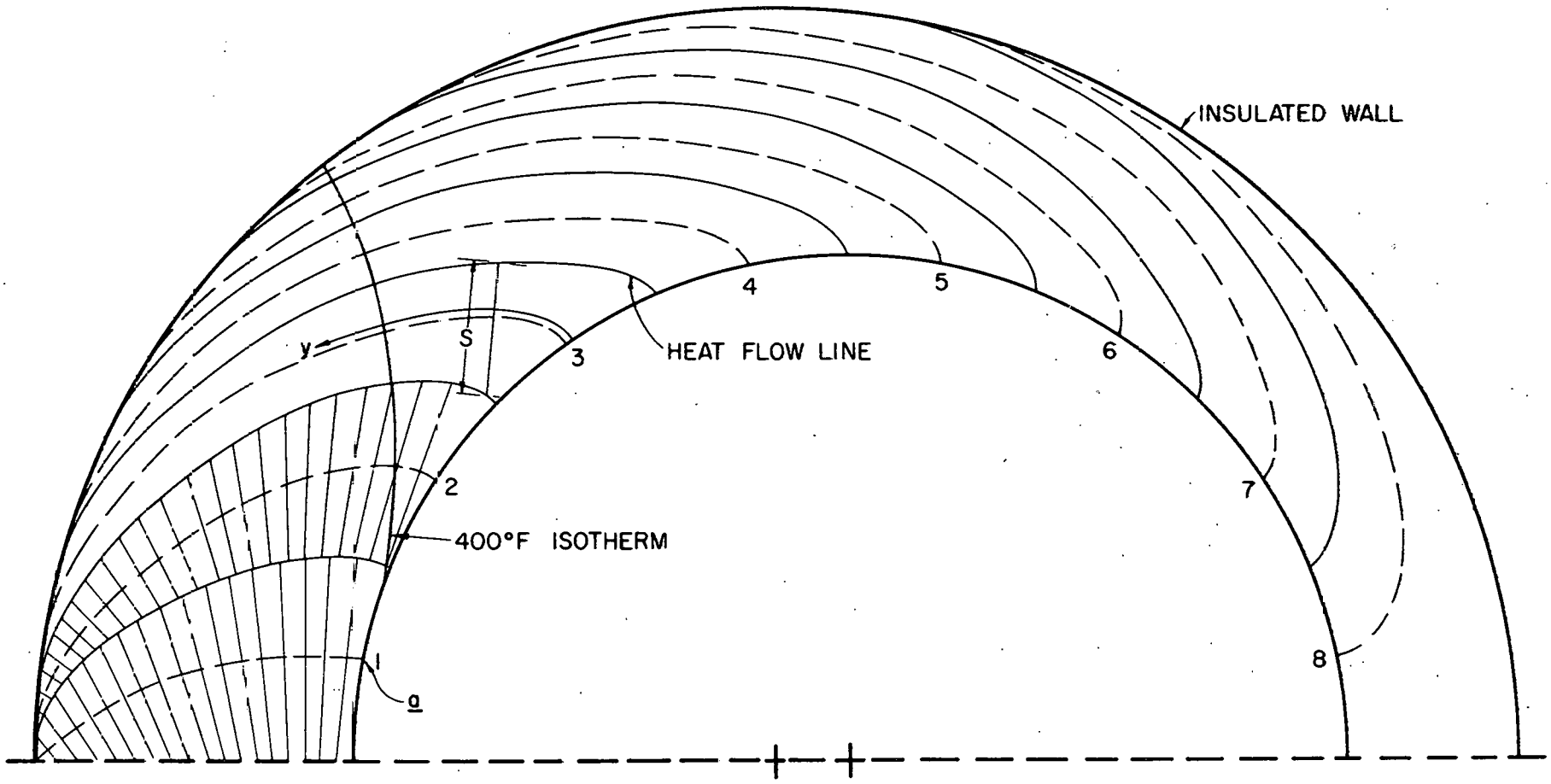

Figure 8 - NUCLEAR SCIENCE & ENGINEERING - Yu and Dwyer

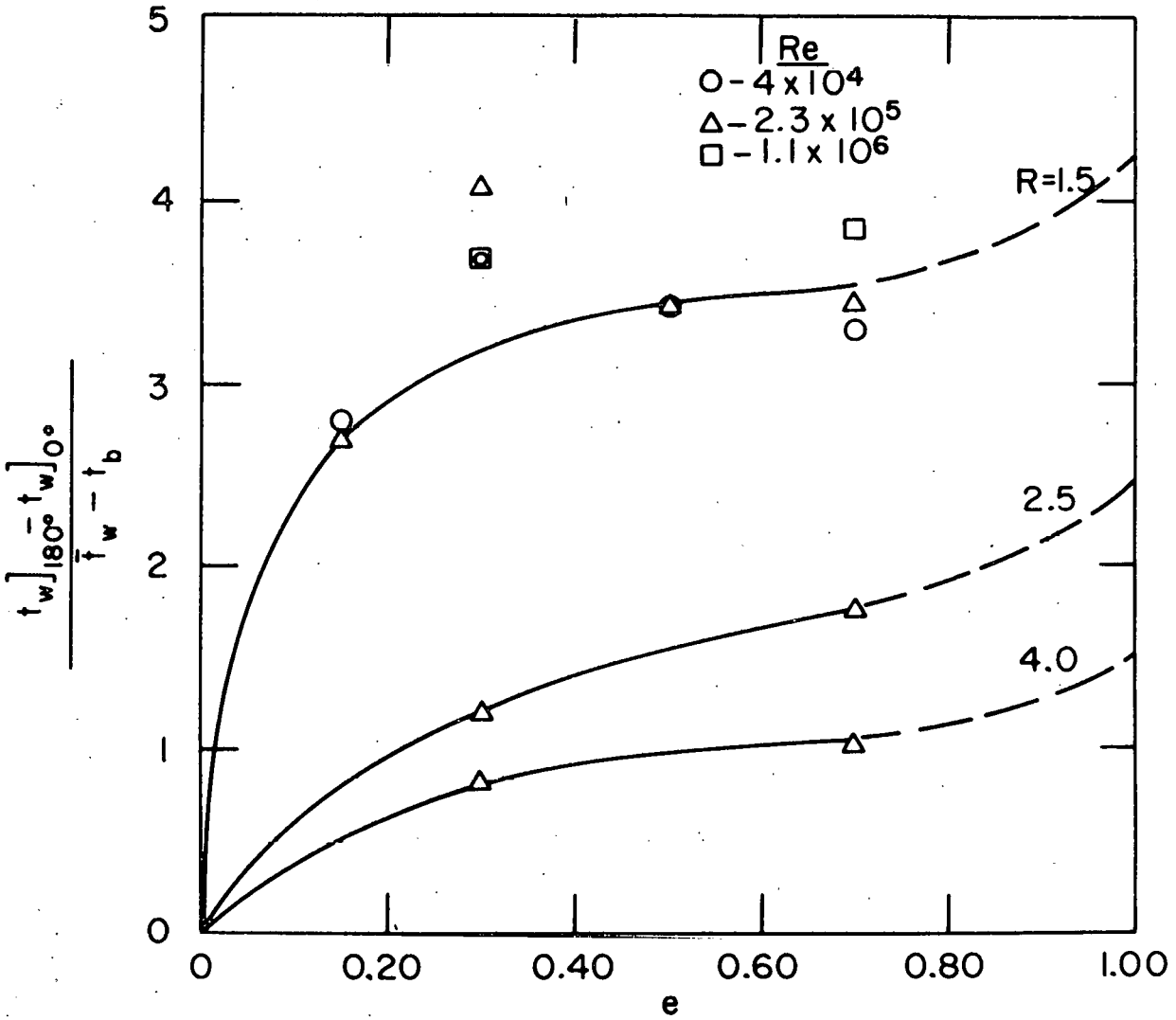

Figure 9 - NUCLEAR SCIENCE & ENGINEERING - Yu and Dwyer

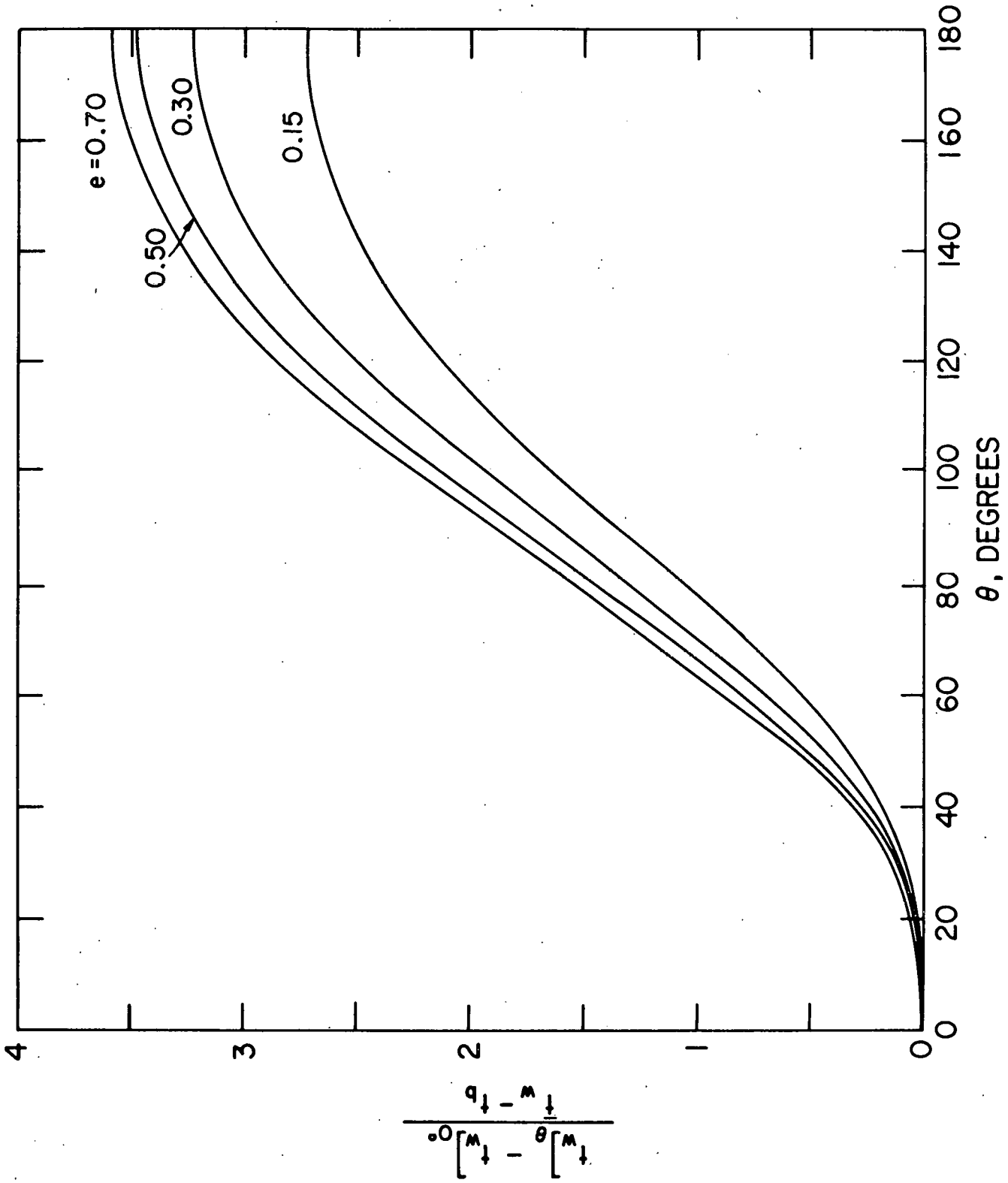

Figure 10 - NUCLEAR SCIENCE & ENGINEERING - Yu and Dwyer

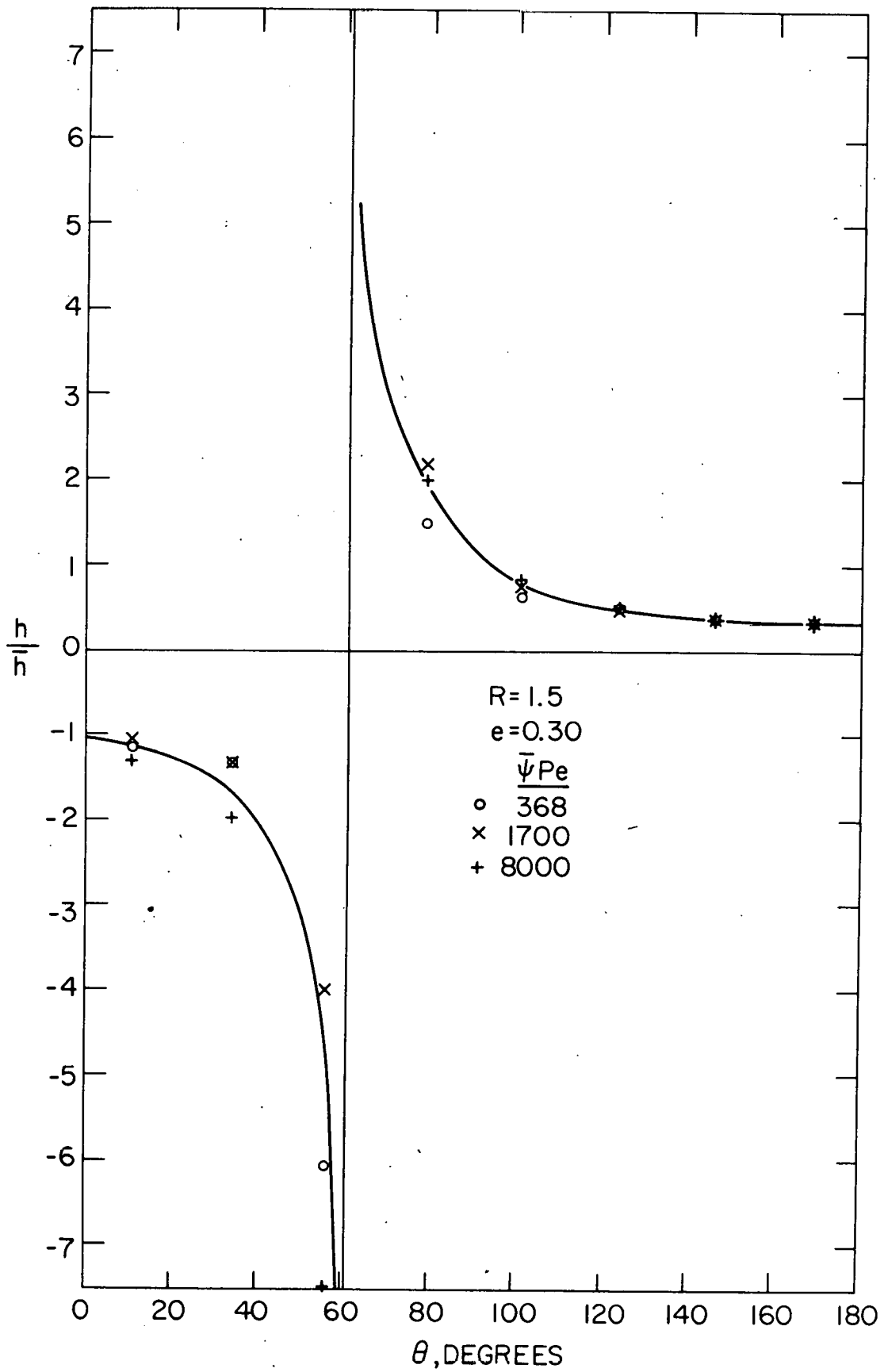

Figure 11 - NUCLEAR SCIENCE & ENGINEERING - Yu and Dwyer

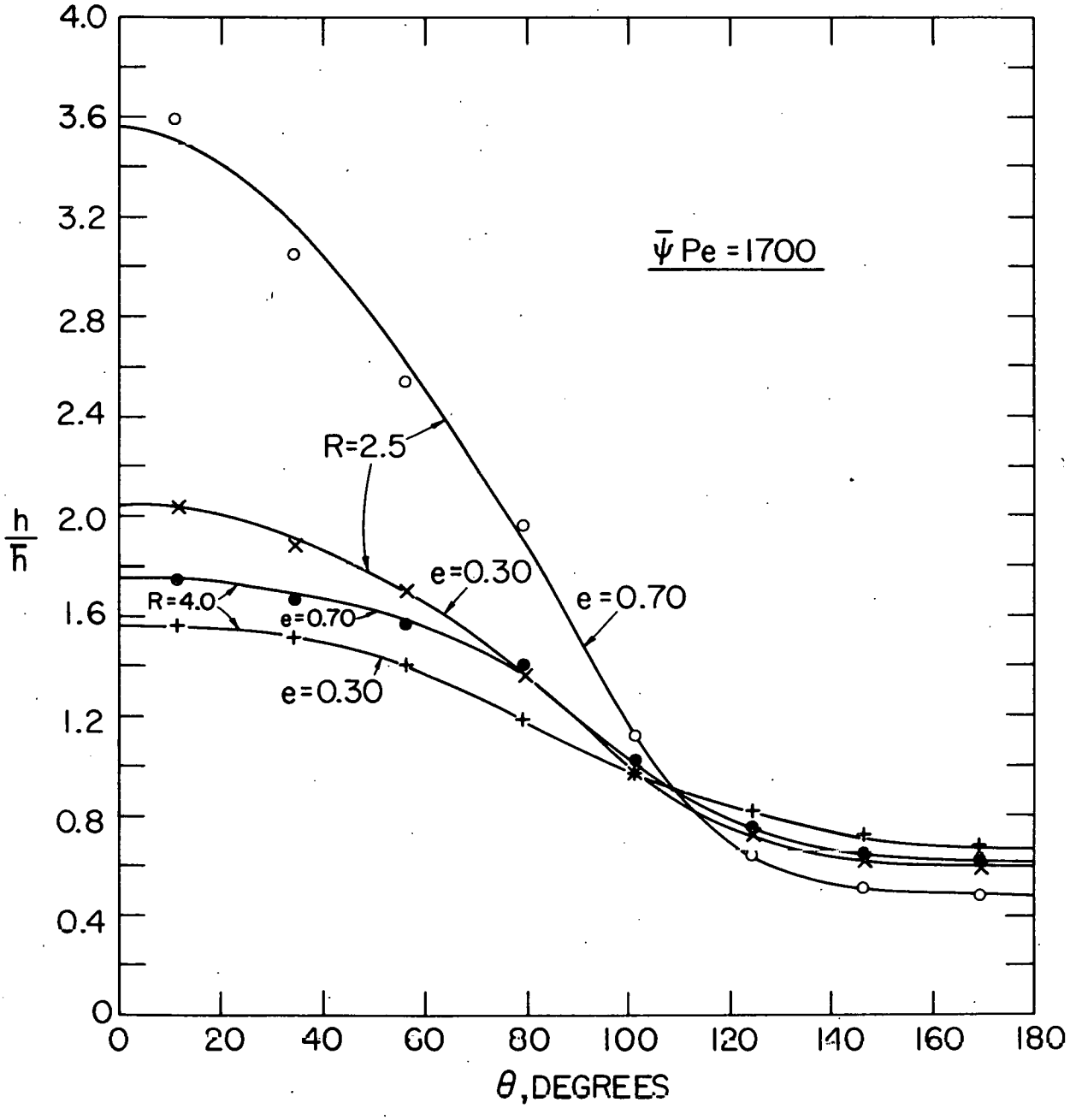

Figure 12 - NUCLEAR SCIENCE & ENGINEERING - Yu and Dwyer

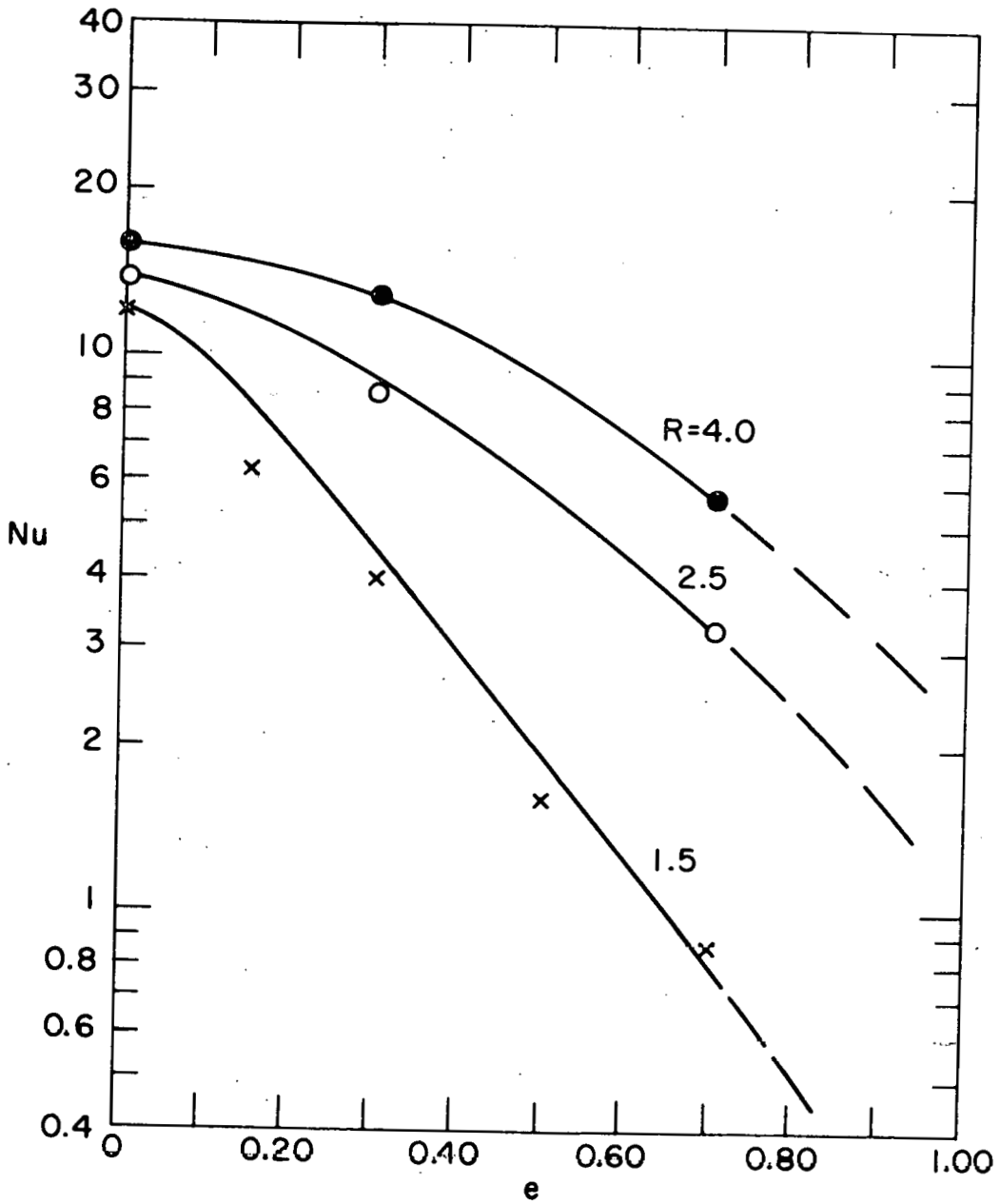

Figure 13 - NUCLEAR SCIENCE & ENGINEERING - Yu and Dwyer

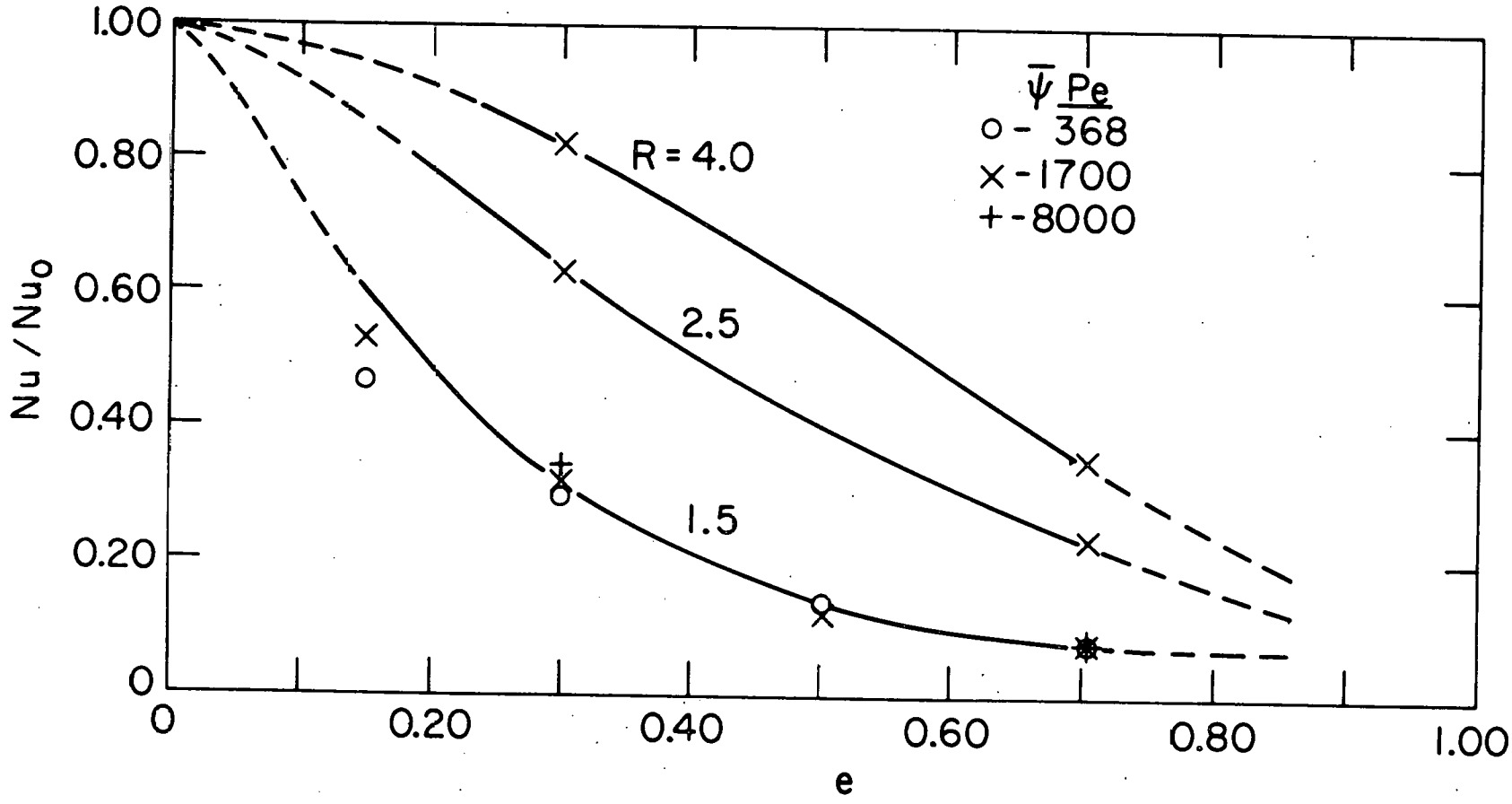

Figure 14 - NUCLEAR SCIENCE & ENGINEERING - Yu and Dwyer

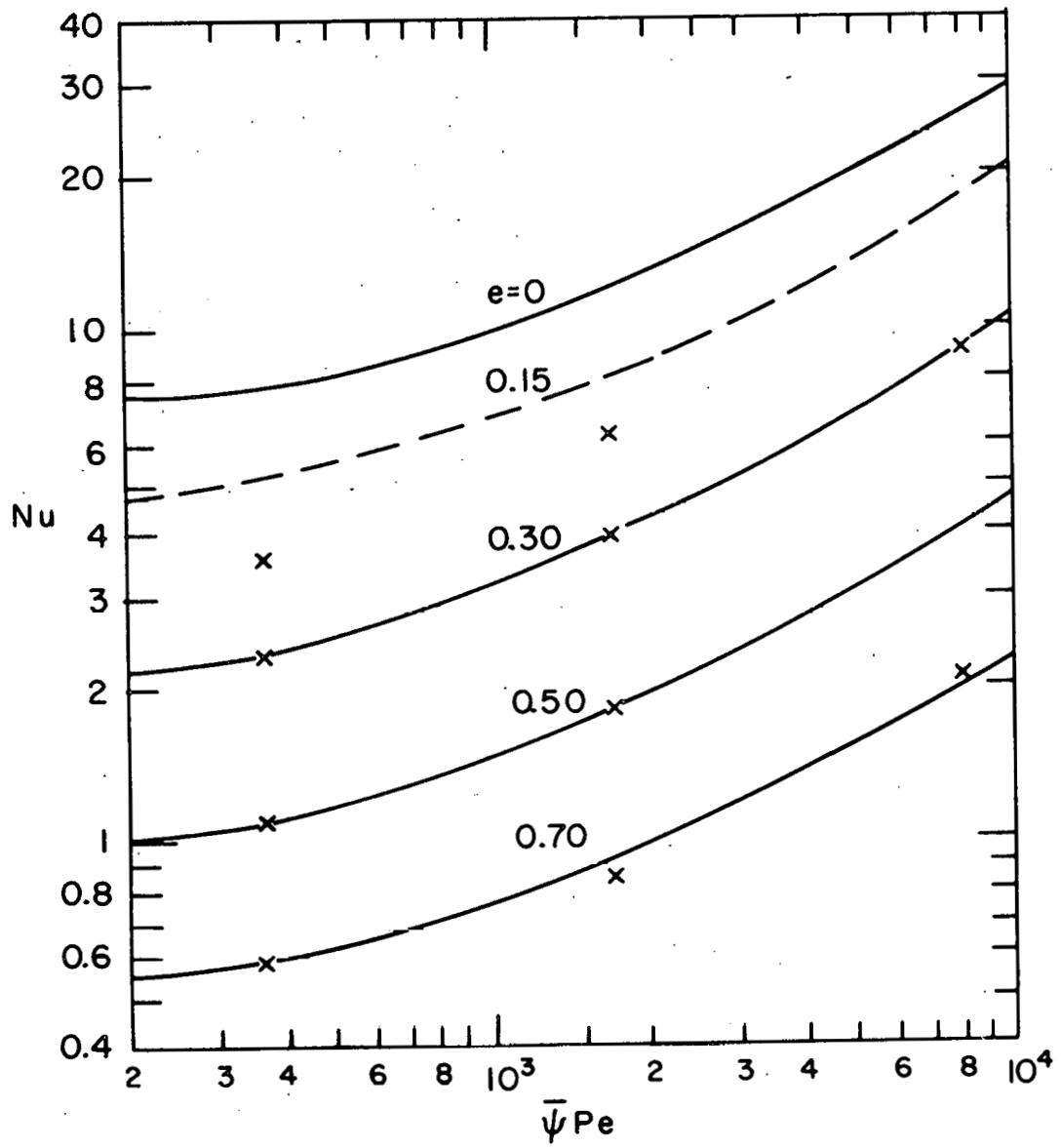

Figure 15 - NUCLEAR SCIENCE & ENGINEERING - Yu and Dwyer

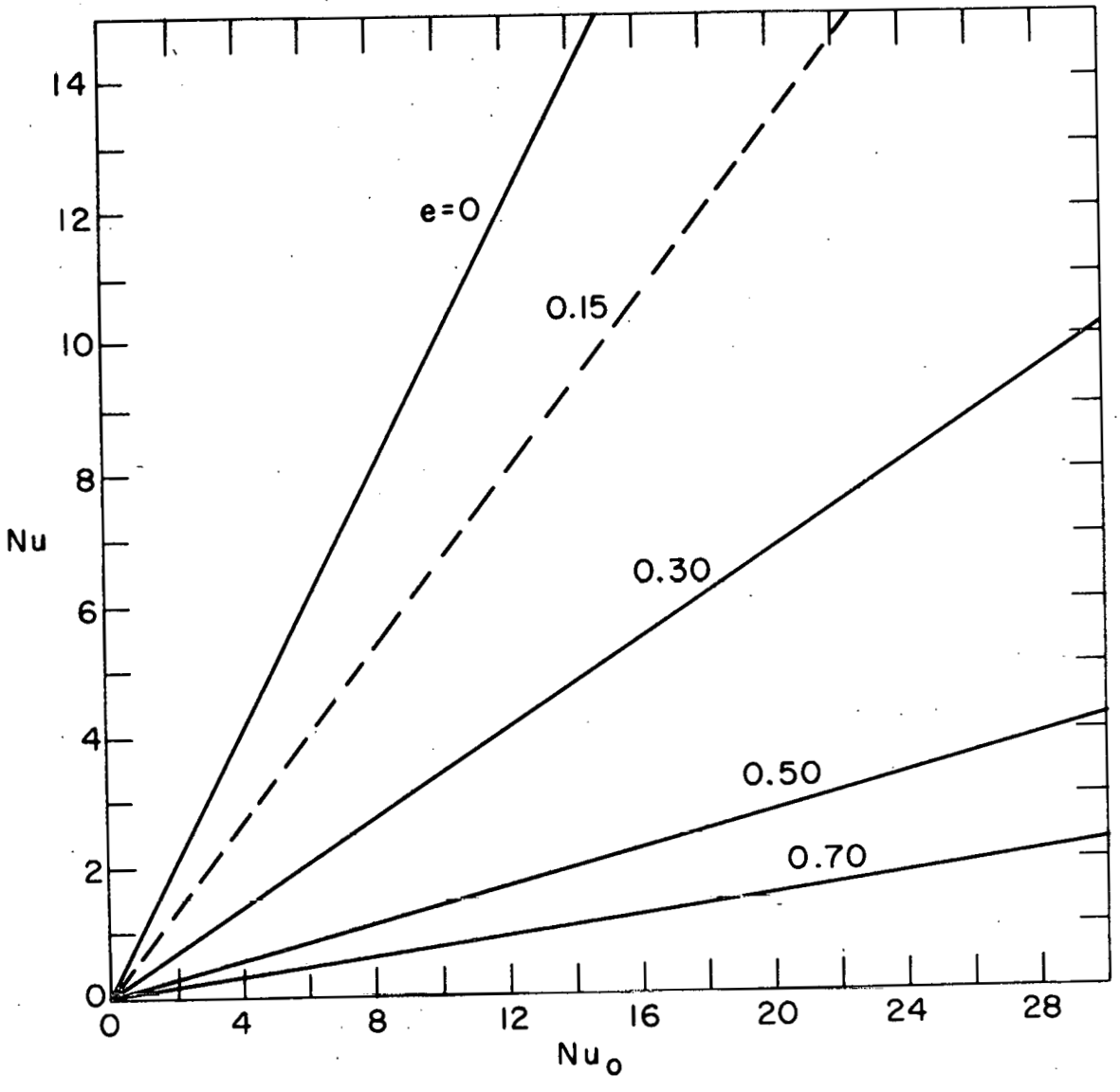

Figure 16 - NUCLEAR SCIENCE & ENGINEERING - Yu and Dwyer

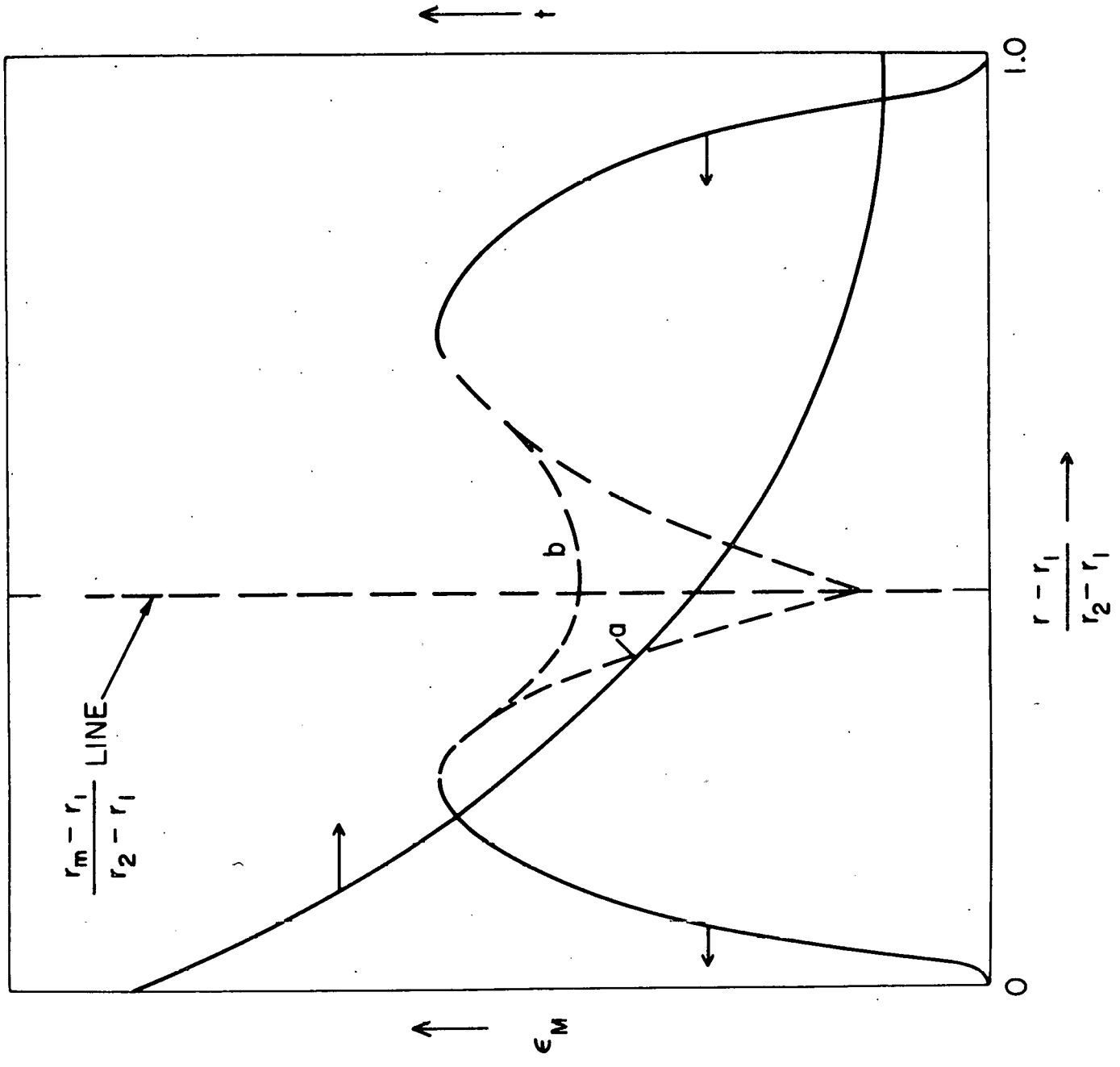

Figure 17 - NUCLEAR SCIENCE & ENGINEERING - Yu and Dwyer